



Current-induced local heating and extractable work in nonthermal vibrational excitationJin-Yi Wang,¹ Zu-Quan Zhang ^{2,*} and Lei-Lei Nian ^{1,†}¹*School of Physics and Astronomy and Yunnan Key Laboratory for Quantum Information, Yunnan University, Kunming 650091, People's Republic of China*²*Department of Physics, Zhejiang Normal University, Jinhua 321004, People's Republic of China*

(Received 19 January 2024; revised 18 April 2024; accepted 13 May 2024; published 4 June 2024)

Electron-vibration interactions in current-carrying nanodevices have been known to induce local heating and nonthermal vibration statistics simultaneously, while theoretical studies so far focus solely on one of them. Based on the quantum master equation, we study vibrationally inelastic electron transport in a double quantum dot device and find that the vibration bunching can be selectively excited for efficient charge and spin transport where the heat generation is inhibited. By introducing the nonequilibrium free energy, the extractable work under a thermal operation from nonthermal vibrations is clearly characterized and quantified. A spin transport channel with large work extraction while maintaining small heat generation rate is found. Furthermore, the extractable work is considerably enhanced by the vibration lasing transition. Our work reveals the relation between current-induced local heating and nonthermal vibration statistics and effects on extractable work, with the aim to control the distribution, storage, and conversion of the heat in nanodevices.

DOI: [10.1103/PhysRevB.109.235402](https://doi.org/10.1103/PhysRevB.109.235402)**I. INTRODUCTION**

Electron transport in biased nanojunctions, such as quantum dots and single molecules, is normally affected by electron-vibration interactions, causing the well-known local heating effect [1–15]. How to control the current-induced local heating (CILH) in nanoelectronics is one of the present-day experimental and theoretical challenges. One of the consequences of the CILH is to increase the effective temperature of the devices, which strongly hinders the mechanical stability [1,16,17]. Removing the heat quickly is the most direct way to reduce the effective temperature, while the existing technologies are difficult to implement [18]. Another effective way is to prevent heat generation by engineering the electronic degrees of freedom [19–31].

In several studies, that have yielded profound insights into the CILH, the vibrations are regarded as a bath, where the vibrations obey the equilibrium Bose distribution [32–35]. By tracing out the electronic system, the average excitation of the vibrational modes is achieved and the CILH is manifested in the nonequilibrium excitation exhibiting a vibrational rectification [36]. Meanwhile, deterministic work from electrons to vibrations, induced by the current-induced force in a nonconservative way, has been observed [37,38]. Based on the nonconservative forces, the current-driven waterwheel or motor is proposed [37,39], where the energy transfer mechanism is obviously different from the stochastic Joule heating [27]. Given the importance of the nonequilibrium vibrations, revealing their statistical properties for low CILH will be essential for nanodevice designs.

When the CILH occurs, electrons lose energy and transfer it to the vibration system; then the probability distribution of the vibration states does not obey the Boltzmann type. It enables the generation of nonthermal vibration statistics, where the emitted vibration is antibunched, coherent, bunched, or superbunched [23,40–43]. Moreover, the extra work may be extracted from the nonthermal vibrations [42,44]. It is, therefore, expected to revisit the CILH from the perspective of the nonthermal statistics. Of particular interest is which vibration state can be used to reduce CILH while still allowing for a significant current and an extractable work.

Here, we study the vibration-mediated electron transport in a biased double quantum dot (DQD) device, as shown in Fig. 1. In contrast to previous works, we include both heat generation and nonthermal statistics. These two nonequilibrium excitations are driven by the same inelastic electron tunneling process and therefore cannot be treated separately. We show that, by simply adjusting the dot energy, the charge and spin transport with low heat generation can be realized when vibration bunching is generated. Meanwhile, the extra work from nonthermal vibration states can be extracted and quantified under a thermal operation, where a spin transport channel with both large work extraction and small heat generation rate is achieved from the superthermal vibration bunching. When the vibration lasing transition is observed, the extractable work is further significantly enhanced. The present connection between nonthermal vibration and extractable work may offer a unique way to explore the CILH from the perspectives of thermodynamics and statistics.

II. MODEL

The system of a DQD with electron-vibration interaction is schematically shown in Fig. 1 and modeled by the

*phyzuquan@zjnu.edu.cn

†llnian@ynu.edu.cn

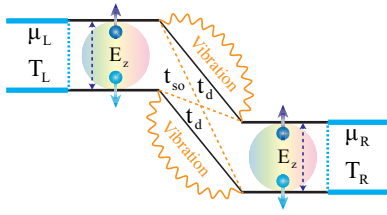


FIG. 1. Schematic of vibrationally inelastic electron transport through a DQD device.

Hamiltonian ($\hbar = 1$)

$$\begin{aligned}
 H = & \sum_{\sigma} \left\{ \sum_{j=1,2} (\varepsilon_j + \tilde{\sigma} E_z/2) d_{j\sigma}^{\dagger} d_{j\sigma} \right. \\
 & \left. + t_d (d_{2\sigma}^{\dagger} d_{1\sigma} + d_{1\sigma}^{\dagger} d_{2\sigma}) \right\} \\
 & + it_{so} \sum_{\sigma, \sigma'} \{ \cos \theta d_{2\sigma}^{\dagger} (\sigma_z)_{\sigma, \sigma'} d_{1\sigma'} + \sin \theta d_{2\sigma}^{\dagger} (\sigma_x)_{\sigma, \sigma'} d_{1\sigma'} \} + \text{H.c.} \\
 & + \sum_{k\sigma v} \varepsilon_{k\sigma v} c_{k\sigma v}^{\dagger} c_{k\sigma v} \\
 & + \sum_{k\sigma} (t_{k\sigma L, 2} c_{k\sigma L}^{\dagger} d_{2\sigma} + t_{k\sigma R, 1} c_{k\sigma R}^{\dagger} d_{1\sigma}) \\
 & + \sum_{k\sigma} (t_{k\sigma L, 2}^* d_{2\sigma}^{\dagger} c_{k\sigma L} + t_{k\sigma R, 1}^* d_{1\sigma}^{\dagger} c_{k\sigma R}) \\
 & + \omega_v a_v^{\dagger} a_v + g \sum_{\sigma} (d_{2\sigma}^{\dagger} d_{2\sigma} - d_{1\sigma}^{\dagger} d_{1\sigma}) (a_v^{\dagger} + a_v) \\
 & + \sum_{\alpha} \omega_{\alpha} a_{\alpha}^{\dagger} a_{\alpha} + \sum_{\alpha} t_{\alpha v} (a_{\alpha}^{\dagger} a_v + a_v^{\dagger} a_{\alpha}), \quad (1)
 \end{aligned}$$

where $d_{j\sigma}^{\dagger}$ is the creation operator of an electron with spin $\sigma = \uparrow, \downarrow$ and energy ε_j in the dot j , with E_z being the Zeeman splitting of the dot level induced by an external magnetic field. Here, $\sigma = \uparrow$ and $\sigma = \downarrow$ correspond to $\tilde{\sigma} = +$ and $\tilde{\sigma} = -$, respectively. The interdot tunneling is allowed with the strength t_d . Due to the spatial confinement of the structures, the Rashba-type spin-orbit coupling is generated [45–50]. The resulting spin-flip strength is t_{so} and θ is the angle between the Zeeman field and the effective spin-orbit field. σ_z and σ_x are the Pauli spin matrix along the z and x axes. The DQD is coupled to two electrodes. $c_{k\sigma v}^{\dagger}$ is the creation operator for an electron with spin σ , momentum k , and energy $\varepsilon_{k\sigma v}$ in the electrode $v = L, R$. $t_{k\sigma v}$ is the tunnel matrix element between the dot and the electrodes. Moreover, we have considered the limit of strong inter- and intradot Coulomb repulsion, such that at a time only one excess electron can be injected from the electrode to the dot. The DQD is also coupled linearly to a local vibration mode of frequency ω_v with electron-vibration coupling constant g . The vibration mode interacts with a thermal bath and $t_{\alpha v}$ is the coupling strength. a_v^{\dagger} and a_{α}^{\dagger} are creation operators for the vibration mode and bath.

When a voltage bias is applied between the two electrodes, an electron can tunnel to dot 2 from electrode L and then tunnels out from dot 1 to electrode R . Depending on the two electronic levels, the electron-vibration coupling may give rise to excitation or deexcitation of the vibrational mode. The

tunneling processes and vibrational excitations remain unchanged as the bias voltage increases. This allows for the limit of high bias voltage and we will focus on this situation in the following. In such a case, the dynamics of the vibration-DQD density matrix ρ can be described by a Markovian master equation [51–53]

$$\begin{aligned}
 \frac{d}{dt} \rho(t) = & -i[H_0, \rho(t)] \\
 & + \sum_{\sigma} \{ \Gamma_{L\sigma} \mathcal{D}[d_{2\sigma}^{\dagger}, \rho(t)] + \Gamma_{R\sigma} \mathcal{D}[d_{1\sigma}, \rho(t)] \} \\
 & + \kappa_v \{ n_B(\omega_v) \mathcal{D}[a_v^{\dagger}, \rho(t)] \\
 & + [1 + n_B(\omega_v)] \mathcal{D}[a_v, \rho(t)] \}, \quad (2)
 \end{aligned}$$

where H_0 is the Hamiltonian of the coupled vibration-DQD system and its coherent evolution is described by the first line. Here, the Hamiltonian H_0 contains three parts: the DQD with $H_D = \sum_{\sigma} \{ \sum_{j=1,2} (\varepsilon_j + \tilde{\sigma} E_z/2) d_{j\sigma}^{\dagger} d_{j\sigma} + t_d (d_{2\sigma}^{\dagger} d_{1\sigma} + d_{1\sigma}^{\dagger} d_{2\sigma}) \} + it_{so} \sum_{\sigma, \sigma'} \{ \cos \theta d_{2\sigma}^{\dagger} (\sigma_z)_{\sigma, \sigma'} d_{1\sigma'} + \sin \theta d_{2\sigma}^{\dagger} (\sigma_x)_{\sigma, \sigma'} d_{1\sigma'} \} + \text{H.c.}$, the vibration mode with $H_v = \omega_v a_v^{\dagger} a_v$, and their coupling with $H_{Dv} = g \sum_{\sigma} (d_{2\sigma}^{\dagger} d_{2\sigma} - d_{1\sigma}^{\dagger} d_{1\sigma}) (a_v^{\dagger} + a_v)$. The second line accounts for the effect of the electrode and $\Gamma_{v\sigma, j}(\varepsilon) = 2\pi \sum_k |t_{k\sigma v, j}|^2 \delta(\varepsilon - \varepsilon_{k\sigma v})$ is the spectral function of the electrode v coupling to dot j with spin σ . The last two lines describe the vibrational heating and cooling induced by the bath and $\kappa_v(\omega) = 2\pi \sum_{\alpha} |t_{\alpha v}|^2 \delta(\omega - \omega_{\alpha})$ being the vibration decay rate. $n_B(\omega) = [\exp(\hbar\omega/k_B T) - 1]^{-1}$ is the Bose-Einstein distribution with the temperature T . For simplicity, $\Gamma_{v\sigma, j}(\varepsilon)$ and $\kappa_v(\omega)$ are assumed to be independent of energy and frequency and we take $\Gamma_{v\sigma, j}(\varepsilon) = \Gamma_{v\sigma}$ and $\kappa_v(\omega) = \kappa_v$. Finally, the superoperator acts according to $\mathcal{D}[A, \rho(t)] = A\rho(t)A^{\dagger} - [A^{\dagger}A\rho(t) + \rho(t)A^{\dagger}A]/2$ for an arbitrary operator A .

To study the spin-dependent transport, the current is defined as $\sum_{v\sigma} I_{v\sigma}(t) = ed\langle N_e \rangle / dt$, where $N_e = \sum_{j\sigma} d_{j\sigma}^{\dagger} d_{j\sigma}$ is the total number of particle operator. In the steady state for $t \rightarrow \infty$, the current flowing from electrode v with spin σ can be written as

$$I_{L\uparrow} = e\Gamma_{L\uparrow} \langle d_{2\uparrow}^{\dagger} d_{2\uparrow} \rangle, I_{L\downarrow} = e\Gamma_{L\downarrow} \langle d_{2\downarrow}^{\dagger} d_{2\downarrow} \rangle, \quad (3)$$

$$I_{R\uparrow} = -e\Gamma_{R\uparrow} \langle d_{1\uparrow}^{\dagger} d_{1\uparrow} \rangle, I_{R\downarrow} = -e\Gamma_{R\downarrow} \langle d_{1\downarrow}^{\dagger} d_{1\downarrow} \rangle. \quad (4)$$

Due to the conservation of charge, the current entering the DQD must be equal to the one leaving it, that is, $I_{L\uparrow} + I_{L\downarrow} = -(I_{R\uparrow} + I_{R\downarrow})$. Then the charge current is given by

$$I_c = -(I_{R\uparrow} + I_{R\downarrow}) \quad (5)$$

and the spin polarization of the current is

$$p_s = \frac{I_{R\uparrow} - I_{R\downarrow}}{I_{R\uparrow} + I_{R\downarrow}}. \quad (6)$$

Note that the spin polarization defined by $I_{L\sigma}$ is always zero when $\Gamma_{L\uparrow} = \Gamma_{L\downarrow}$. When the electron moves from left to right, the current-induced heat generation Q_h can be characterized by the energy transfer from electron to vibration system. From the time evolution of the average value of $H_v = \omega_v a_v^{\dagger} a_v$, one

gets

$$\frac{d\langle H_v \rangle}{dt} = J_v(t) + Q_h(t), \quad (7)$$

where $J_v(t)$ is the energy flux from the bath to the vibration mode. In the steady state, $Q_h(t)$ becomes

$$Q_h = -ig\omega_v \left\langle \sum_{\sigma} (d_{2\sigma}^{\dagger} d_{2\sigma} - d_{1\sigma}^{\dagger} d_{1\sigma})(a_v^{\dagger} - a_v) \right\rangle. \quad (8)$$

We assume that the temperatures of electrons and vibrations are the same; then heat generation is solely driven by an electron residing on the DQD. Meanwhile, the vibration mode can be excited by this electron and, consequently, the nonthermal vibration statistics are observed. Thus the statistical properties of the vibration mode have to be considered together with the heat generation. To this end, the equal-time second-order correlation function, $g_v^{(2)}(0) = \langle a_v^{\dagger} a_v^{\dagger} a_v a_v \rangle / \langle a_v^{\dagger} a_v \rangle^2$, is introduced to characterize the vibration statistics. For $g = 0$, the vibration mode is in a thermal state with $g_v^{(2)}(0) = 2$. For $g \neq 0$, the nonthermal states with antibunched, coherent, bunched, and superthermal vibration emissions may be achieved, which are characterized by $g_v^{(2)}(0) < 1$, $g_v^{(2)}(0) = 1$, $1 < g_v^{(2)}(0) < 2$, and $g_v^{(2)}(0) > 2$. In numerical calculations, we focus on the weak electron-vibration coupling, $g \sim 0.3\omega_v$, which has been verified by employing a modified Born-Markov quantum master equation [54–56].

Previously, most studies have primarily focused on the impact of heat generation on the stability of devices [1,16,17]. For example, in single-molecule devices, the heat generation may lead to the breaking of chemical bonds [57]. To measure the heating or cooling effect of a device, an effective temperature has been introduced [2,3,5,6,8,15,19,58–60]. When the effective temperature increases, the vibration populations are distinct from those observed under equilibrium conditions, which are determined by the thermal bath. Consequently, the single effective temperature is not sufficient to describe the nonthermal vibration states and additional quantities such as free energy and entropy are needed [42]. In such a case, the extra work can be extracted from the nonthermal vibrations [42,44]. Moreover, it is established that the proportional relationship between the current and the heat generation does not hold in nanodevices [32–34]. Inspired by this, we will reveal how to strike a balance between the current, heat generation, and extractable work under nonthermal vibration excitation.

III. CHARGE TRANSPORT

We first consider the case $E_z = 0$ and $t_{so} = 0$; then the spin-up and spin-down channels are completely degenerate and indistinguishable, resulting in a spin-independent transport. Figure 2(a) shows the charge current I_c as a function of the energy difference $\varepsilon_d = \varepsilon_2 - \varepsilon_1$. For $g = 0$, the electron transport is dominated by an elastic channel and a resonant peak is observed at $\varepsilon_d = 0$. For a finite g , away from this resonance, a series of sidepeaks appear at $\varepsilon_d = n\omega_v$ ($n \geq 1$), which corresponds to the vibration-assisted tunneling [54–56]. The equal-time second-order correlation function $g_v^{(2)}(0)$ is shown in Fig. 2(b); for $g = 0$ the vibration mode is only coupled to a

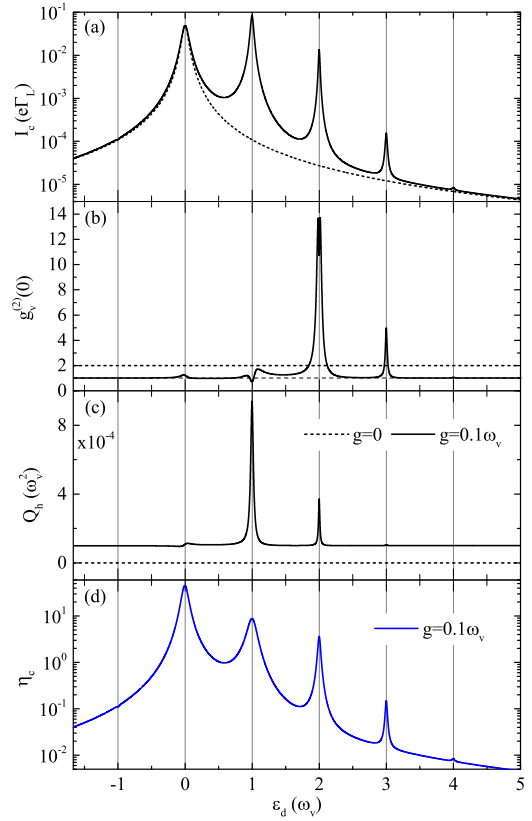


FIG. 2. Charge current I_c (a), equal-time second-order correlation function $g_v^{(2)}(0)$ (b), heat generation Q_h (c), and charge quality factor η_c (d) as a function of energy difference ε_d for indicated values of electron-vibration coupling strength g . Other parameters are $\omega_v = 0.3$ eV, $\kappa_v = 0.01\omega_v$, $T = 0.1\omega_v$, $\Gamma_{L\sigma} = 0.01\omega_v$, $\Gamma_{R\sigma} = 0.001\omega_v$, $t_d = 0.033\omega_v$, $t_{so} = 0$, $E_z = 0$, and $\theta = \pi/2$.

thermal bath, yielding $g_v^{(2)}(0) = 2$. When the vibration mode is excited by the tunneling electron ($g \neq 0$), it can exhibit nonthermal statistics with $g_v^{(2)}(0) \neq 2$. The heat generation Q_h at $\varepsilon_d = \omega_v$ has a maximum, while it has a minimum around $\varepsilon_d = 0$, as shown in Fig. 2(c). Thus the heat generation can be significantly inhibited when the vibration mode is in a bunched state. Since the electron contributes differently to I_c and Q_h , the relative magnitudes of the peaks in I_c do not coincide with those in Q_h [32–34]. Thus it is difficult to measure the “optimal region” (high I_c with low Q_h) for device operation. For this, we can define a quality factor as

$$\eta_c = \frac{I_c}{Q_h}, \quad (9)$$

where $\eta_c \rightarrow \infty$ means an ideal operation induced by $Q_h = 0$ with a significant I_c . As expected, a high value of η_c is achieved at $\varepsilon_d = 0$ [Fig. 2(d)], indicating the low heat generation rate.

In Fig. 3 we show the impact of electron-vibration coupling g on I_c , $g_v^{(2)}(0)$, Q_h , and η_c for different energy differences ε_d . At $\varepsilon_d = 0$, I_c remains almost unaffected by g [Fig. 3(a)]. As g increases, the inelastic channel starts to contribute to I_c at $\varepsilon_d = n\omega_v$ ($n = 1, 2, 3$). Eventually at large g , the inelastic part in I_c becomes dominant and therefore the vibration bunching

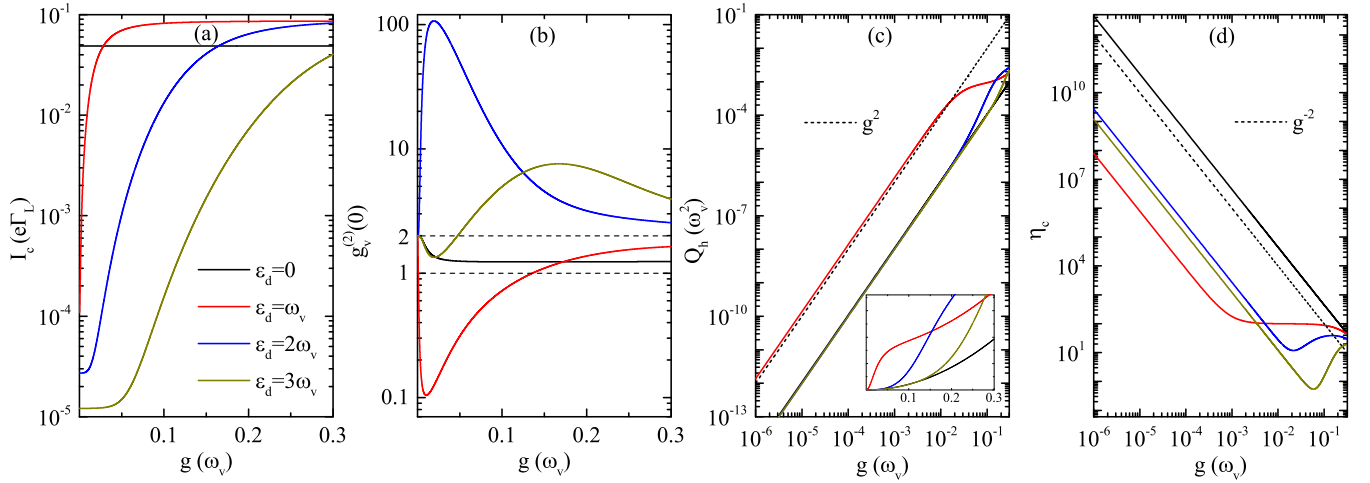


FIG. 3. Charge current I_c (a), equal-time second-order correlation function $g_v^{(2)}(0)$ (b), heat generation Q_h (c), and charge quality factor η_c (d) as a function of electron-vibration coupling strength g for indicated values of energy difference ε_d . The inset in (c) shows Q_h in a linear scale. Same parameters as in Fig. 2.

or superthermal bunching is observed [Fig. 3(b)]. The heat generation at $\varepsilon_d = 0$ is, however, lower as compared to the case of $\varepsilon_d = n\omega_v$. This indicates that, although the large coupling to the vibration mode can enhance the heat generation, it may not change the contribution rate on the channel at $\varepsilon_d = 0$ in Q_h [Fig. 3(c)]. As a consequence, η_c is always larger at $\varepsilon_d = 0$ than at $\varepsilon_d = n\omega_v$. We can therefore claim that the device operation is benign when the vibration bunching occurs.

Furthermore, in the region of small g ($g < 10^{-3}\omega_v$), the linear dependence of Q_h on g with a log-log scale is observed. To reveal such a behavior, the expression of Q_h in Eq. (8) can be further expanded by

$$\begin{aligned} \frac{d\langle d_{2\sigma}^\dagger d_{2\sigma} a_v^\dagger \rangle}{dt} = & -it_d \langle (d_{2\sigma}^\dagger d_{1\sigma} - d_{1\sigma}^\dagger d_{2\sigma}) a_v^\dagger \rangle \\ & + \left(i\omega_v - \frac{\kappa_v}{2} \right) \langle d_{2\sigma}^\dagger d_{2\sigma} a_v^\dagger \rangle \\ & + ig \langle d_{2\sigma}^\dagger d_{2\sigma} \rangle + \Gamma_{L\sigma} \langle d_{2\sigma} d_{2\sigma}^\dagger a_v^\dagger \rangle, \end{aligned} \quad (10)$$

$$\begin{aligned} \frac{d\langle d_{1\sigma}^\dagger d_{1\sigma} a_v^\dagger \rangle}{dt} = & -it_d \langle (d_{1\sigma}^\dagger d_{2\sigma} - d_{2\sigma}^\dagger d_{1\sigma}) a_v^\dagger \rangle \\ & + \left(i\omega_v - \Gamma_{R\sigma} - \frac{\kappa_v}{2} \right) \langle d_{1\sigma}^\dagger d_{1\sigma} a_v^\dagger \rangle \\ & - ig \langle d_{1\sigma}^\dagger d_{1\sigma} \rangle, \end{aligned} \quad (11)$$

and $\langle d_{j\sigma}^\dagger d_{j\sigma} a_v \rangle = [\langle d_{j\sigma}^\dagger d_{j\sigma} a_v^\dagger \rangle]^\dagger$, which allow us to write the steady-state Q_h as

$$\begin{aligned} Q_h = & -ig\omega_v \left\{ 4it_d \operatorname{Re} \left(\left[\frac{1}{(i\omega_v - \frac{\kappa_v}{2})} + \frac{1}{(i\omega_v - \Gamma_R - \frac{\kappa_v}{2})} \right] \right. \right. \\ & \left. \left. \times \langle (d_2^\dagger d_1 - d_1^\dagger d_2) a_v^\dagger \rangle \right) \right\} \end{aligned}$$

$$\begin{aligned} & - 4\Gamma_L \operatorname{Im} \left(\frac{1}{(i\omega_v - \frac{\kappa_v}{2})} \langle d_2 d_2^\dagger a_v^\dagger \rangle \right) \\ & + 2ig \left[\frac{\kappa_v}{\omega_v^2 + (\frac{\kappa_v}{2})^2} \langle d_2^\dagger d_2 \rangle + \frac{2\Gamma_R + \kappa_v}{\omega_v^2 + (\Gamma_R + \frac{\kappa_v}{2})^2} \langle d_1^\dagger d_1 \rangle \right] \Bigg\}, \end{aligned} \quad (12)$$

where $\langle d_i^\dagger d_j \rangle = \langle d_{i\sigma}^\dagger d_{j\sigma} \rangle$ and $\Gamma_v = \Gamma_{v\sigma}$. For small g , we can approximately decouple electrons from vibrations, where $\langle (d_2^\dagger d_1 - d_1^\dagger d_2) a_v^\dagger \rangle$ and $\langle d_2 d_2^\dagger a_v^\dagger \rangle$ can be replaced with $\langle (d_2^\dagger d_1 - d_1^\dagger d_2) \rangle \langle a_v^\dagger \rangle$ and $\langle d_2 d_2^\dagger \rangle \langle a_v^\dagger \rangle$. In such a case, the vibration mode is weakly excited; thus no significant vibration population can build up in it. Then Q_h is dominated by the last line in Eq. (12) and we can safely omit the terms that involve $\langle (d_2^\dagger d_1 - d_1^\dagger d_2) a_v^\dagger \rangle$ and $\langle d_2 d_2^\dagger a_v^\dagger \rangle$. These two approximations are equivalent. To obtain an analytical expression for Q_h , we need to calculate $\langle d_1^\dagger d_1 \rangle$ and $\langle d_2^\dagger d_2 \rangle$, and their forms are similar to those for $g = 0$. With the normalization condition for the diagonal reduced-density matrix elements in the electron system, $\langle d_2 d_2^\dagger \rangle + 2\langle d_1^\dagger d_1 \rangle + 2\langle d_2^\dagger d_2 \rangle = 1$, and for $\varepsilon_d = 0$ one can get

$$\langle d_1^\dagger d_1 \rangle = \frac{2t_d^2 \Gamma_L}{\Gamma_R^2 \Gamma_L + 8t_d^2 \Gamma_L + 2t_d^2 \Gamma_R}, \quad (13)$$

$$\langle d_2^\dagger d_2 \rangle = \frac{(\Gamma_R^2 + 4t_d^2) \Gamma_L}{2[\Gamma_R^2 \Gamma_L + 8t_d^2 \Gamma_L + 2t_d^2 \Gamma_R]}. \quad (14)$$

Taking into account the parameters in Fig. 3, then Q_h , in turn, is given by

$$Q_h \approx \frac{4g^2 (\Gamma_R + \kappa_v) \Gamma_L}{\omega_v (4\Gamma_L + \Gamma_R)}. \quad (15)$$

The detailed derivation is provided in Appendix A of Supplemental Material Ref. [61] and the results obtained using the analytical Eq. (15) agree well with the numerical solutions. As a consequence, Eq. (15) follows that the dependence of $Q_h \propto g^2$ and thus $\eta_c \propto g^{-2}$ holds clearly, as verified in Figs. 3(c) and 3(d).

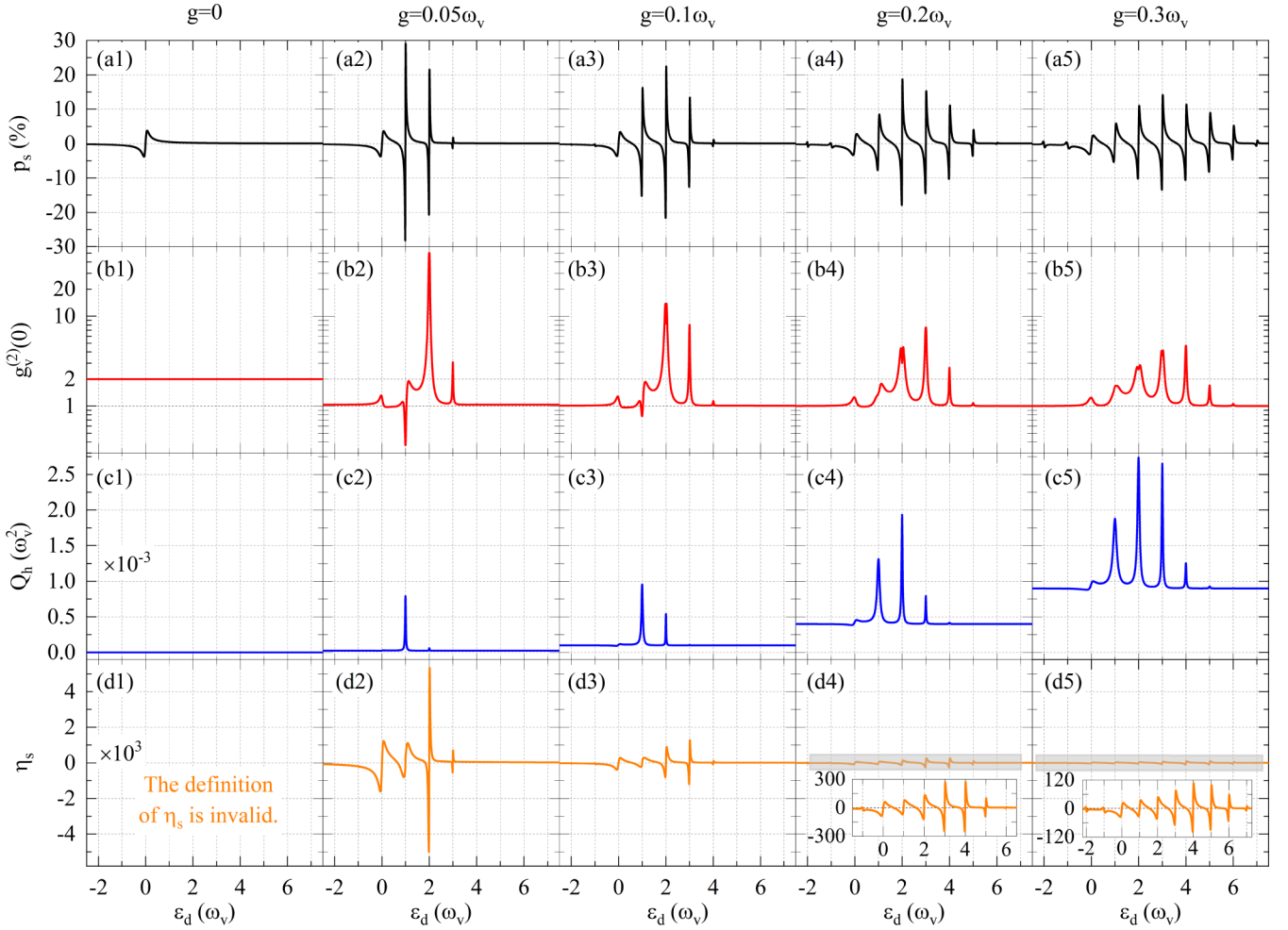


FIG. 4. Spin polarization p_s (a), equal-time second-order correlation function $g_v^{(2)}(0)$ (b), heat generation Q_h (c), and spin quality factor η_s (d) as a function of energy difference ε_d for indicated values of electron-vibration coupling strength g and for $t_{so} = 0.033\omega_v$ and $E_z = 0.005\omega_v$. The definition of η_s only works for $g \neq 0$; thus it is invalid in (d1). The insets in (d4) and (d5) show the enlarged views of the shaded areas. Same parameters as in Fig. 2.

IV. SPIN TRANSPORT

In Fig. 4(a), we show the spin polarization p_s as a function of the energy difference ε_d in the presence of the Zeeman splitting E_z and the spin-orbit coupling t_{so} . Then the two spin channels are no longer degenerate and the spin flip processes occur. The left electrode acts as an electron source; thus $I_{L\uparrow} = I_{L\downarrow}$ due to $\Gamma_{L\uparrow} = \Gamma_{L\downarrow}$. A spin degenerate electron will tunnel into the dot 2 from the left electrode, due to the spin flip; it then tunnels out from dot 1 to the right electrode with a finite spin polarization. One can see that p_s at $\varepsilon_d \approx 0$ is rather small, even for large g , while it increases significantly in the vibration-assisted regions with $\varepsilon_d \approx n\omega_v$. Thus the nonthermal vibrations, except the bunching at $\varepsilon_d \approx 0$, can be selectively excited for high p_s [Fig. 4(b)]. Figure 4(c) presents Q_h as a function of ε_d for different g . In the absence of the electron-vibration coupling, $g = 0$, the heat generation vanishes. When $g \neq 0$, Q_h exhibits a peak at a certain ε_d , which depends on g . The larger the electron-vibration coupling g is, the more peaks there will be in Q_h , due to the multivibration excitation. Meanwhile, increasing g can shift the maximum value of Q_h to where the value of ε_d is larger. As p_s is not

proportional to Q_h , we can introduce $\eta_s (= p_s/Q_h)$, which is similar to η_c , into our consideration. There is always a minimum in Q_h for $\varepsilon_d \approx 0$, similarly as the case for $E_z = 0$ and $t_{so} = 0$ in Fig. 2(c). However, different from I_c , the peak value of p_s at $\varepsilon_d \approx 0$ is clearly smaller than that at $\varepsilon_d \approx n\omega_v$ for a given g . As a result, η_s achieves a relatively high value at $\varepsilon_d \approx 2\omega_v$, where the superthermal vibration bunching is observed.

All the above quantities of interest are shown in Fig. 5 as a function of g . When g increases, p_s decreases monotonically for $\varepsilon_d \approx 0$, while it first increases and then decreases for $\varepsilon_d \approx n\omega_v$. For $g \lesssim 1.3 \times 10^{-3}\omega_v$, p_s at $\varepsilon_d \approx 0$ is larger than that at $\varepsilon_d \approx n\omega_v$, while Q_h , in turn, concerns the opposite situation. Thus η_s can reach its maximum value at $\varepsilon_d \approx 0$. This is similar to that in Fig. 3. For $g > 1.3 \times 10^{-3}\omega_v$, depending on g , p_s with $\varepsilon_d \approx n\omega_v$ becomes enhanced and eventually surpasses the ones for $\varepsilon_d \approx 0$. Since the minimum value of Q_h always appears at $\varepsilon_d \approx 0$, then the dominant contribution to η_s can become the transport channel at $\varepsilon_d \approx n\omega_v$, such as $n = 2$ and $n = 3$ with $g_v^{(0)}(0) \approx 45$ and $g_v^{(0)}(0) \approx 5$. Obviously, compared with charge transport, we can achieve a high η_s for large g in spin transport when the vibration superbunching is observed. Additionally, the dependence of $Q_h \propto g^2$ and $\eta_s \propto g^{-2}$

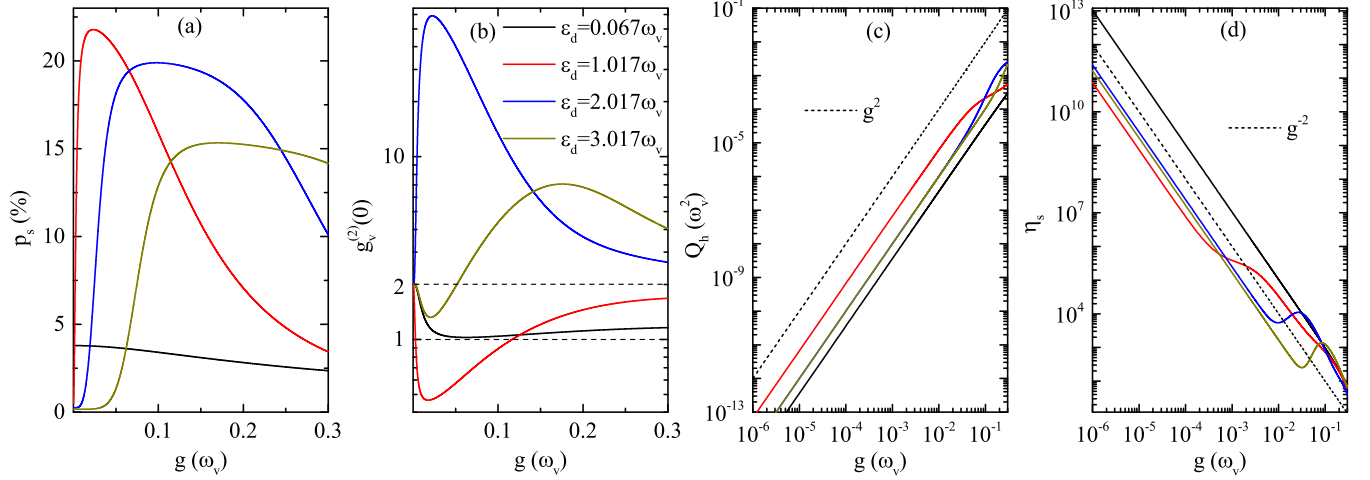


FIG. 5. Spin polarization p_s (a), equal-time second-order correlation function $g_v^{(2)}(0)$ (b), heat generation Q_h (c), and spin quality factor η_s (d) as a function of electron-vibration coupling strength g for indicated values of energy difference ε_d . Same parameters as in Fig. 4.

for small g is also found, as explained in Figs. 3(c) and 3(d). Note that the dot energy we choose in Fig. 5 is shifted a little away from the vibration energy $n\omega_v$, which is solely to ensure that p_s takes a positive value. When we take $\varepsilon_d = n\omega_v$, a high value of η_s for $n = 2$ or $n = 3$ is also obtained (Appendix B of Supplemental Material Ref. [61]).

V. EFFECT OF TEMPERATURE

Let us now study how the temperature affects the above physical quantities. For the low temperatures, an electron injected from the left electrode occupies dot 2, it can relax to dot 1 with the emission of a vibration, and thus the vibration-emission-assisted transport occurs at $\varepsilon_d > 0$. In such a case, the thermal bath can only absorb vibrations; then the energy transfers from electron to vibration system in one direction, yielding $Q_h > 0$. For higher temperatures, it can be immediately seen that the charge current I_c and spin polarization p_s apart from the part at $\varepsilon_d > 0$ corresponding to the vibration emission includes also the electron tunneling processes at $\varepsilon_d < 0$ originating from the vibration absorption [Figs. 6(a) and 6(b)]. For $\varepsilon_d < 0$, the tunneling process is as follows. An electron can tunnel to dot 2 from the left electrode, as the energy level of dot 1 is higher than the dot 2; then the electron tunneling from dot 2 to 1 is only allowed by absorbing a vibration. This is caused by the energy transfer from vibration to electron system, where the energy source is the thermal bath. The energy flux from the bath can be obtained from Eq. (7) and is of the form

$$J_v = \omega_v \kappa_v \{n_B(\omega_v) \langle a_v a_v^\dagger \rangle - [n_B(\omega_v) + 1] \langle a_v^\dagger a_v \rangle\}, \quad (16)$$

where J_v consists of two terms—the first term corresponds to the energy loss, while the second term corresponds to the energy absorption. The vibration mode can be excited by the bath when the former occurs, and the vibration-absorption-assisted transport is observed at $\varepsilon_d = -\omega_v$ and consequently the vibration cooling with $Q_h < 0$ and $g_v^{(2)}(0) \approx 2$ [Fig. 6(c)]. As a result, the heat generation vanishes ($Q_h = 0$) between the cooling and the heating and $\eta_{c,s} \rightarrow \infty$ is achieved for the ideal operation of the device. At $\varepsilon_d = -\omega_v$, $Q_h = 0$ at room

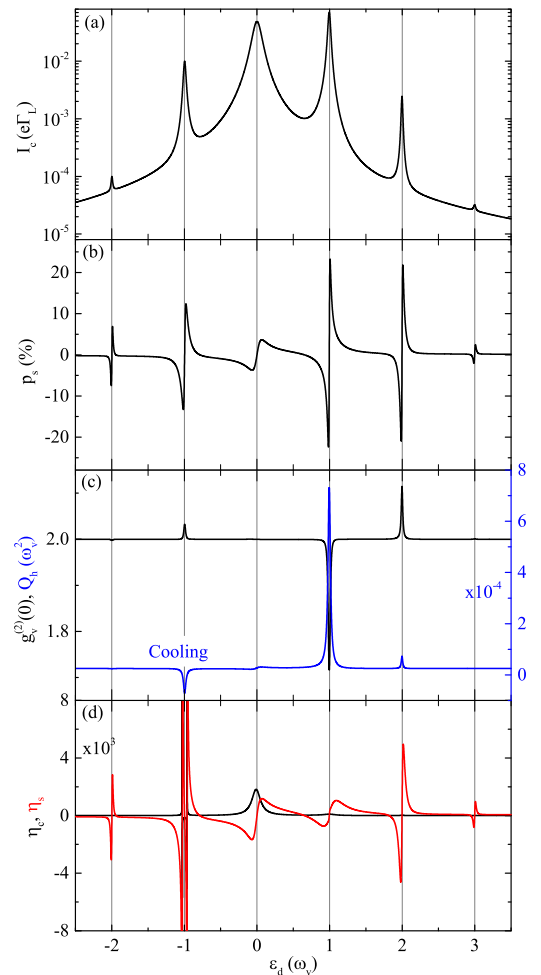


FIG. 6. (a), (b) Charge current I_c and spin polarization p_s as a function of energy difference ε_d for $T = 0.5\omega_v$. (c), (d) Similar to (a), but for equal-time second-order correlation function $g_v^{(2)}(0)$, heat generation Q_h , charge quality factor η_c , and spin quality factor η_s versus ε_d . Same parameters as in Fig. 4.

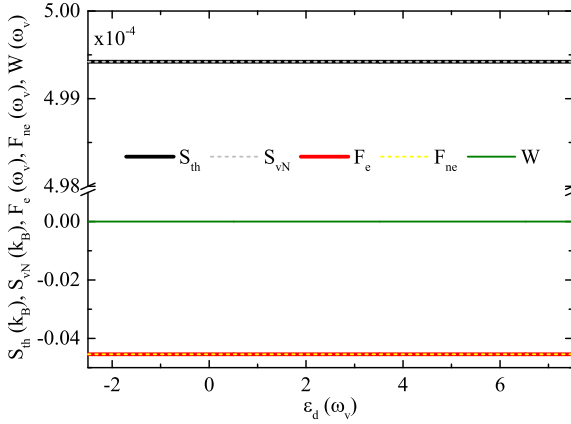


FIG. 7. Thermal entropy S_{th} , von Neumann entropy S_{vN} , equilibrium free energy F_e , nonequilibrium free energy F_{ne} , and extractable work W as a function of energy difference ε_d for $g = 0$. Same parameters as in Fig. 2.

temperature $T = 0.026$ eV is also accessible when we take $\omega_v = 52$ meV.

VI. EXTRACTABLE WORK

One of the most intuitive consequences of the presence of electron-vibration coupling is an effective increase of the energy and entropy of the vibrational degrees of freedom, accompanied by the generation of nonthermal vibration statistics. In principle, the useful work can be extracted from a nonthermal vibration [42,44,62,63], which is treated as a battery. To quantify the extractable work, the entropy, free energy, and internal energy are introduced to characterize the nonthermal states of the vibrations. For $g = 0$, the vibration mode is in a thermal state and we can use effective thermal entropy [$S_{\text{th}} = k_B \{(\langle a_v^\dagger a_v \rangle + 1) \ln(\langle a_v^\dagger a_v \rangle + 1) - \langle a_v^\dagger a_v \rangle \ln \langle a_v^\dagger a_v \rangle\}$] and equilibrium free energy $F_e = -k_B T \ln \text{Tr}\{\exp(-H_v/k_B T)\}$ as a reference point. For comparison, the von Neumann entropy (S_{vN}) and nonequilibrium free energy (F_{ne}) are given by

$$S_{\text{vN}} = -k_B \text{Tr}\{\rho_v \ln \rho_v\}, \quad (17)$$

$$F_{\text{ne}} = U - T S_{\text{vN}}, \quad (18)$$

where $\rho_v = \text{Tr}_e\{\rho\}$ is the density matrix of the vibration system and its internal energy is $U = \text{Tr}\{H_v \rho_v\}$. As expected, $S_{\text{vN}} = S_{\text{th}}$ and $F_{\text{ne}} = F_e$ in Fig. 7 are observed for thermal vibrations. Under a thermal operation, the maximum extractable work is defined as

$$W = F_{\text{ne}} - F_e, \quad (19)$$

where $g = 0$ leads to $W = 0$ and $W \neq 0$ is achieved when the vibration mode is in a nonthermal state. In Fig. 8, we present the von Neumann entropy S_{vN} and extractable work W as a function of the electron-vibration coupling g for different ε_d . When g is increased, S_{vN} in Fig. 8(a) strongly deviates from S_{th} , indicating the appearance of the nonthermal vibrations, particularly in the vibration-assisted regime. The extractable work in Fig. 8(b), in turn, is relatively large at $\varepsilon_d = \omega_v$ ($\varepsilon_d = 2\omega_v$) in the small (large) coupling regime and rather small at $\varepsilon_d = 0$ in the whole region. For the charge transport, as discussed in Figs. 2 and 3, the bunched vibration

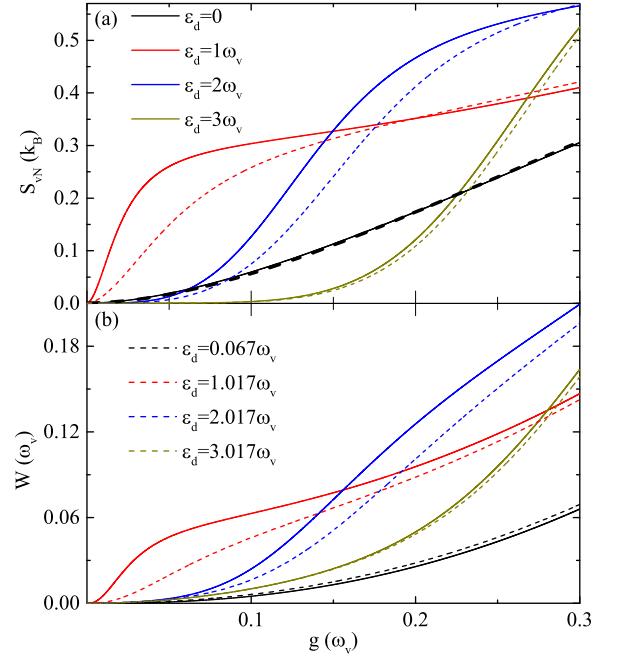


FIG. 8. (a) Entropy S_{vN} as a function of electron-vibration coupling g for indicated values of energy difference ε_d . (b) Similar to (a), but for extractable work W versus g . Parameters for solid and dashed lines are the same as in Figs. 3 and 5, respectively.

at $\varepsilon_d = 0$ is chosen for high η_c , while the extractable work is less pronounced in comparison to the vibrations in $\varepsilon_d = n\omega_v$. Interestingly, the generation of the superthermal bunching in spin transport (Figs. 4 and 5) is to identify the vibration state with a sufficiently high η_s , where the extractable work becomes also pronounced.

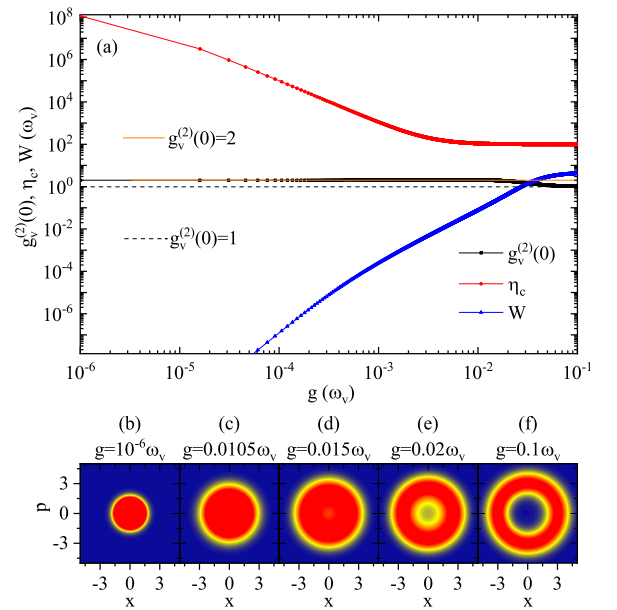


FIG. 9. (a) Equal-time second-order correlation function $g_v^{(2)}(0)$, charge quality factor η_c , and extractable work W as a function of electron-vibration coupling g . (b)–(f) Wigner functions for $g = 10^{-6}\omega_v$, $g = 0.0105\omega_v$, $g = 0.015\omega_v$, $g = 0.02\omega_v$, and $g = 0.1\omega_v$, respectively. Same parameters as in Fig. 2.

VII. VIBRATION LASING TRANSITION

When the vibration lasing transition occurs, the von Neumann entropy markedly deviates from the thermal entropy, thereby obtaining significant extractable work [42,44]. To achieve the lasing transition, small dissipation of the vibration mode is required; then we take $\kappa_v = 10^{-4}\omega_v$. In this regime, we present g dependence of $g_v^{(2)}(0)$, η_c , and W for $\varepsilon_d = \omega_v$ in Fig. 9(a). For small g , the weak coupling to electrons results in the thermal state of the vibration mode with $g_v^{(2)}(0) = 2$. Above a certain threshold of the electron-vibration coupling, the vibration lasing situation is observed, due to the population inversion between the two electronic levels, indicated by $g_v^{(2)}(0) = 1$. As shown in Figs. 9(b)–9(f), the vibration excitation can also be visualized in the Wigner distribution functions for different g . It clearly shows the transition of the vibration state from thermal to coherent, which manifests itself as an evolution from blob to ring structure in the Wigner function. From Figs. 3(d) and 8(b), we can achieve $\eta_c \approx 10^2$ and $W \approx 0.06\omega_v$ for $g = 0.1\omega_v$ and $\varepsilon_d = \omega_v$, while in Fig. 9(a) $\eta_c \approx 10^2$ and $W \approx 5\omega_v$. Therefore, while maintaining η_c , W can be further enhanced when the vibration lasing occurs and similarly for the spin transport (Appendix C of Supplemental Material Ref. [61]).

VIII. CONCLUSIONS

We have studied the vibration-mediated electron transport in a double quantum dot attached to two electrodes and found that the heat generation can be significantly suppressed in the charge and spin channels when the vibration bunching appears. Moreover, the nonthermal vibration mode can serve as a battery and the extractable work from it can be quantified by the nonequilibrium free energy. Among all the nonthermal vibration states, the large work extraction with small heat generation rate from the superthermal bunching is identified in the spin transport channel. The extractable work can be further enhanced when the vibration lasing transition occurs.

ACKNOWLEDGMENTS

The work was supported by the National Natural Science Foundation of China (Grants No. 12204405 and No. 12204416) and by the Yunnan Fundamental Research Project (Grants No. 202301AT070108 and No. 202401AW070005).

-
- [1] J. Gaudio, L. J. Lauhon, and W. Ho, Vibrationally mediated negative differential resistance in a single molecule, *Phys. Rev. Lett.* **85**, 1918 (2000).
- [2] Y.-C. Chen, M. Zwolak, and M. Di Ventra, Local heating in nanoscale conductors, *Nano Lett.* **3**, 1691 (2003).
- [3] Z. Huang, B. Xu, Y. Chen, M. D. Ventra, and N. Tao, Measurement of current-induced local heating in a single molecule junction, *Nano Lett.* **6**, 1240 (2006).
- [4] J.-T. Lü and J.-S. Wang, Coupled electron and phonon transport in one-dimensional atomic junctions, *Phys. Rev. B* **76**, 165418 (2007).
- [5] Z. Huang, F. Chen, R. D'agosta, P. A. Bennett, M. Di Ventra, and N. Tao, Local ionic and electron heating in single-molecule junctions, *Nat. Nanotechnol.* **2**, 698 (2007).
- [6] M. Galperin, M. A. Ratner, and A. Nitzan, Molecular transport junctions: vibrational effects, *J. Phys.: Condens. Matter* **19**, 103201 (2007).
- [7] J.-S. Wang, J. Wang, and J. T. Lü, Quantum thermal transport in nanostructures, *Eur. Phys. J. B* **62**, 381 (2008).
- [8] M. Tsutsui, M. Taniguchi, and T. Kawai, Local heating in metal-molecule-metal junctions, *Nano Lett.* **8**, 3293 (2008).
- [9] Y. Dubi and M. Di Ventra, Colloquium: Heat flow and thermoelectricity in atomic and molecular junctions, *Rev. Mod. Phys.* **83**, 131 (2011).
- [10] N. Li, J. Ren, L. Wang, G. Zhang, P. Hänggi, and B. Li, Colloquium: Phononics: Manipulating heat flow with electronic analogs and beyond, *Rev. Mod. Phys.* **84**, 1045 (2012).
- [11] Y. Wang and Z. Xu, The critical power to maintain thermally stable molecular junctions, *Nat. Commun.* **5**, 4297 (2014).
- [12] L. Cui, R. Miao, C. Jiang, E. Meyhofer, and P. Reddy, Perspective: Thermal and thermoelectric transport in molecular junctions, *J. Chem. Phys.* **146**, 092201 (2017).
- [13] F. Evers, R. Korytár, S. Tewari, and J. M. van Ruitenbeek, Advances and challenges in single-molecule electron transport, *Rev. Mod. Phys.* **92**, 035001 (2020).
- [14] T. E. Li, B. Cui, J. E. Subotnik, and A. Nitzan, Molecular polaritonics: chemical dynamics under strong light-matter coupling, *Annu. Rev. Phys. Chem.* **73**, 43 (2022).
- [15] Q. Meng, J. Zhang, Y. Zhang, W. Chu, W. Mao, Y. Zhang, J. Yang, Y. Luo, Z. Dong, and J. G. Hou, Local heating and raman thermometry in a single molecule, *Sci. Adv.* **10**, ead11015 (2024).
- [16] H. Park, J. Park, A. K. Lim, E. H. Anderson, A. P. Alivisatos, and P. L. McEuen, Nanomechanical oscillations in a single-C₆₀ transistor, *Nature (London)* **407**, 57 (2000).
- [17] G. Schulze, K. J. Franke, A. Gagliardi, G. Romano, C. S. Lin, A. L. Rosa, T. A. Niehaus, T. Frauenheim, A. Di Carlo, A. Pecchia, and J. I. Pascual, Resonant electron heating and molecular phonon cooling in single C₆₀ junctions, *Phys. Rev. Lett.* **100**, 136801 (2008).
- [18] E. Pop, S. Sinha, and K. E. Goodson, Heat generation and transport in nanometer-scale transistors, *Proc. IEEE* **94**, 1587 (2006).
- [19] M. Galperin, A. Nitzan, and M. A. Ratner, Heat conduction in molecular transport junctions, *Phys. Rev. B* **75**, 155312 (2007).
- [20] M. Galperin, K. Saito, A. V. Balatsky, and A. Nitzan, Cooling mechanisms in molecular conduction junctions, *Phys. Rev. B* **80**, 115427 (2009).
- [21] R. Härtle, C. Benesch, and M. Thoss, Vibrational nonequilibrium effects in the conductance of single molecules with multiple electronic states, *Phys. Rev. Lett.* **102**, 146801 (2009).
- [22] G. Romano, A. Gagliardi, A. Pecchia, and A. Di Carlo, Heating and cooling mechanisms in single-molecule junctions, *Phys. Rev. B* **81**, 115438 (2010).
- [23] R. Härtle and M. Thoss, Vibrational instabilities in resonant electron transport through single-molecule junctions, *Phys. Rev. B* **83**, 125419 (2011).

- [24] J.-T. Lü, M. Brandbyge, P. Hedegård, T. N. Todorov, and D. Dundas, Current-induced atomic dynamics, instabilities, and raman signals: Quasiclassical langevin equation approach, *Phys. Rev. B* **85**, 245444 (2012).
- [25] L. Simine and D. Segal, Vibrational cooling, heating, and instability in molecular conducting junctions: full counting statistics analysis, *Phys. Chem. Chem. Phys.* **14**, 13820 (2012).
- [26] J.-T. Lü, H. Zhou, J.-W. Jiang, and J.-S. Wang, Effects of electron-phonon interaction on thermal and electrical transport through molecular nano-conductors, *AIP Adv.* **5**, 053204 (2015).
- [27] J.-T. Lü, R. B. Christensen, J.-S. Wang, P. Hedegård, and M. Brandbyge, Current-induced forces and hot spots in biased nanojunctions, *Phys. Rev. Lett.* **114**, 096801 (2015).
- [28] R. Härtle, C. Schinabeck, M. Kulkarni, D. Gelbwaser-Klimovsky, M. Thoss, and U. Peskin, Cooling by heating in nonequilibrium nanosystems, *Phys. Rev. B* **98**, 081404(R) (2018).
- [29] D. Segal and B. K. Agarwalla, Vibrational heat transport in molecular junctions, *Annu. Rev. Phys. Chem.* **67**, 185 (2016).
- [30] J.-T. Lü, B.-Z. Hu, P. Hedegård, and M. Brandbyge, Semi-classical generalized langevin equation for equilibrium and nonequilibrium molecular dynamics simulation, *Prog. Surf. Sci.* **94**, 21 (2019).
- [31] R. J. Preston, T. D. Honeychurch, and D. S. Kosov, Cooling molecular electronic junctions by ac current, *J. Chem. Phys.* **153**, 121102 (2020).
- [32] Q. F. Sun and X. C. Xie, Heat generation by electric current in mesoscopic devices, *Phys. Rev. B* **75**, 155306 (2007).
- [33] J. Liu, J. Song, Q. F. Sun, and X. C. Xie, Electric-current-induced heat generation in a strongly interacting quantum dot in the coulomb blockade regime, *Phys. Rev. B* **79**, 161309(R) (2009).
- [34] L.-L. Zhou, S. S. Li, J. N. Wei, and S. Q. Wang, Characteristics of heat generation in a quantum dot, *Phys. Rev. B* **83**, 195303 (2011).
- [35] Q. Chen, L.-M. Tang, K.-Q. Chen, and H.-K. Zhao, Heat generated by electrical current in a mesoscopic system perturbed by alternating current fields, *J. Appl. Phys.* **114**, 084301 (2013).
- [36] R. Härtle and M. Thoss, Resonant electron transport in single-molecule junctions: Vibrational excitation, rectification, negative differential resistance, and local cooling, *Phys. Rev. B* **83**, 115414 (2011).
- [37] D. Dundas, E. J. McEniry, and T. N. Todorov, Current-driven atomic waterwheels, *Nat. Nanotechnol.* **4**, 99 (2009).
- [38] J.-T. Lü, M. Brandbyge, and P. Hedegård, Blowing the fuse: Berry's phase and runaway vibrations in molecular conductors, *Nano Lett.* **10**, 1657 (2010).
- [39] R. Bustos-Marún, G. Refael, and F. von Oppen, Adiabatic quantum motors, *Phys. Rev. Lett.* **111**, 060802 (2013).
- [40] S. Takei, Y. B. Kim, and A. Mitra, Enhanced fano factor in a molecular transistor coupled to phonons and luttinger-liquid leads, *Phys. Rev. B* **72**, 075337 (2005).
- [41] X. Zhong and J. C. Cao, Interference effects on vibration-mediated tunneling through interacting degenerate molecular states, *J. Phys.: Condens. Matter* **21**, 295602 (2009).
- [42] T. Wang, L.-L. Nian, and J.-T. Lü, Nonthermal vibrations in biased molecular junctions, *Phys. Rev. E* **102**, 022127 (2020).
- [43] L.-L. Nian, L. Bai, and S. Hu, Vibration squeezing and its detection in a single molecular junction, *Phys. Rev. B* **107**, 245428 (2023).
- [44] O. Culhane, M. T. Mitchison, and J. Goold, Extractable work in quantum electromechanics, *Phys. Rev. E* **106**, L032104 (2022).
- [45] F. Mireles and G. Kirczenow, Ballistic spin-polarized transport and rashba spin precession in semiconductor nanowires, *Phys. Rev. B* **64**, 024426 (2001).
- [46] F. Kuemmeth, S. Ilani, D. Ralph, and P. McEuen, Coupling of spin and orbital motion of electrons in carbon nanotubes, *Nature (London)* **452**, 448 (2008).
- [47] J. Birkholz and V. Meden, Spin-orbit coupling effects in one-dimensional ballistic quantum wires, *J. Phys.: Condens. Matter* **20**, 085226 (2008).
- [48] J. E. Birkholz and V. Meden, Spin-polarized currents through interacting quantum wires with nonmagnetic leads, *Phys. Rev. B* **79**, 085420 (2009).
- [49] S. Droste, S. Andergassen, and J. Splettstoesser, Josephson current through interacting double quantum dots with spin-orbit coupling, *J. Phys.: Condens. Matter* **24**, 415301 (2012).
- [50] L. L. Nian, L. Zhang, F.-R. Tang, L. P. Xue, R. Zhang, and L. Bai, Spin-resolved Andreev transport through a double quantum-dot system: Role of the rashba spin-orbit interaction, *J. Appl. Phys.* **115**, 213704 (2014).
- [51] G. Lindblad, On the generators of quantum dynamical semigroups, *Commun. Math. Phys.* **48**, 119 (1976).
- [52] H.-P. Breuer and F. Petruccione, *The Theory of Open Quantum Systems* (Oxford University Press on Demand, Oxford, 2002).
- [53] H. J. Carmichael, *Statistical Methods in Quantum Optics I: Master Equations and Fokker-Planck Equations* (Springer Science & Business Media, New York, 2013).
- [54] T. Brandes and N. Lambert, Steering of a bosonic mode with a double quantum dot, *Phys. Rev. B* **67**, 125323 (2003).
- [55] N. Lambert and F. Nori, Detecting quantum-coherent nanomechanical oscillations using the current-noise spectrum of a double quantum dot, *Phys. Rev. B* **78**, 214302 (2008).
- [56] C. Wang, J. Ren, B. Li, and Q.-H. Chen, Quantum transport of double quantum dots coupled to an oscillator in arbitrary strong coupling regime, *Eur. Phys. J. B* **85**, 110 (2012).
- [57] H. Li, T. A. Su, V. Zhang, M. L. Steigerwald, C. Nuckolls, and L. Venkataraman, Electric field breakdown in single molecule junctions, *J. Am. Chem. Soc.* **137**, 5028 (2015).
- [58] Z. Ioffe, T. Shamai, A. Ophir, G. Noy, I. Yutsis, K. Kfir, O. Cheshnovsky, and Y. Selzer, Detection of heating in current-carrying molecular junctions by raman scattering, *Nat. Nanotechnol.* **3**, 727 (2008).
- [59] D. R. Ward, D. A. Corley, J. M. Tour, and D. Natelson, Vibrational and electronic heating in nanoscale junctions, *Nat. Nanotechnol.* **6**, 33 (2011).
- [60] D. Zhang, X. Zheng, and M. Di Ventra, Local temperatures out of equilibrium, *Phys. Rep.* **830**, 1 (2019).
- [61] See Supplemental Material at <http://link.aps.org/supplemental/10.1103/PhysRevB.109.235402> for verification of Eq. (15), spin transport for $\varepsilon_d = n\omega_v$, and vibration lasing transition in spin transport.
- [62] V. Vedral, The role of relative entropy in quantum information theory, *Rev. Mod. Phys.* **74**, 197 (2002).
- [63] M. Esposito and C. Van den Broeck, Second law and landauer principle far from equilibrium, *Europhys. Lett.* **95**, 40004 (2011).